

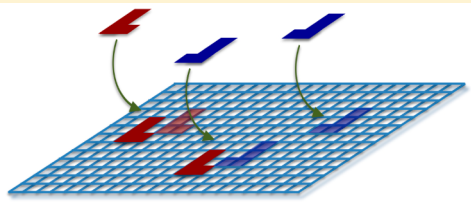
Monte Carlo Simulations of the Uptake of Chiral Compounds on Solid Surfaces

Stavros Karakalos[†] and Francisco Zaera^{*‡}

Department of Chemistry and UCR Center for Catalysis, University of California, Riverside, California 92521, United States

ABSTRACT: A Monte Carlo algorithm was developed and used to describe and explain previous experimental results associated with the kinetics of the uptake of chiral molecules on solid surfaces. The specific system simulated in this study is the adsorption of propylene oxide (PO) on Pt(111) surfaces. The surface was represented by a square lattice, and the time evolution of the adsorption, starting from a clean surface, was simulated via a number of sequential events chosen using a stochastic approach based on the so-called Master equation and derived from the formalism advanced by Gillespie.

Two main assumptions were required to explain the experimental results: (1) that adsorption is assisted by previously adsorbed molecules, that is, that the probability for sticking is higher next to other adsorbates than on empty isolated sites, and (2) that the geometry adopted by the new adsorbate next to an old one is defined and different for homochiral versus heterochiral pairs. Our model was able to quantitatively reproduce the experimental data and to explain a number of important observations associated with the fact that the adsorbates are chiral, including the following: (1) the final PO saturation depends on the enantiocomposition of the gas phase, yielding a layer approximately 20% less dense with a racemic mixture than with enantiopure S-PO or R-PO; (2) the same changes in saturation coverages are seen if PO of different chirality are dosed sequentially; (3) the sticking probability is also higher with enantiopure adsorbates, at least in the initial stages of the uptake; (4) the sticking probability initially increases with increasing exposure, until reaching a maximum at about 20% of saturation; and (5) the adsorbed layers do not show any long-range ordering but display small linear clusters. It was also possible to reproduce the experimental observation that the addition of a prochiral molecule such as propylene (Py) to a surface dosed with a small amount of a chiral “seed” (PO) leads to an amplification of the initial enantioselectivity of that surface.



1. INTRODUCTION

The kinetics of chemical reactions on solid surfaces are central to many areas of practical importance, including catalysis, electrochemistry, tribology, film deposition, crystallization, and etching, yet they are often difficult to describe. This is because the methodology used to analyze most chemical kinetics in homogeneous media are not adequate to address the additional complications introduced by the presence of a surface, which include a change in dimensionality (from 3D to 2D), possible strong interactions among adsorbed reactants (and products), which can be long-range, and spatial heterogeneity in the way the different species are distributed on the surface.^{1,2} These issues are not easy to emulate using simple rate laws, and typically cannot be reproduced using conventional microkinetics or mean-field kinetic models.^{3–6} Instead, they can be visualized by using a stochastic approach, specifically employing Monte Carlo algorithms.^{7–13} Here we describe the use of such an approach to develop a molecular-level understanding of the adsorption of chiral (and prochiral) molecules on solid surfaces.

The adsorption of chiral molecules on solid surfaces, which can define enantioselectivity in catalysis, crystallization, and chemical separation techniques, presents some unique and interesting challenges.^{14–16} Recent surface-science studies have shown that the enantiocomposition of adsorbed layers of chiral compounds may be quite different than that of the gas or liquid from which they are made,^{17–19} and can also be manipulated via the introduction of small amounts of “seed” agents.^{20,21}

Although many of the trends seen in these chiral surface systems may be explained in terms of thermodynamics,²² there are examples where kinetics may be the dominant effect.¹⁹ This is certainly the case for the early stages of the adsorption of propylene oxide on Pt(111) single crystal surfaces, a prototypical system being characterized in our laboratory.^{19,21,23,24} Our experimental data, obtained by using a combination of temperature-programmed desorption (TPD), molecular beams, and scanning tunneling microscopy (STM), are complemented here with the use of Monte Carlo kinetic simulations to identify the factors that explain the enantiobiases observed and reported in previous publications.

We show that Monte Carlo simulations can be quite useful in explaining the kinetics of the adsorption of chiral molecules. First, we were able to reproduce the uptake of propylene oxide (PO) on Pt(111), and to explain the changes in saturation coverage seen with variations in the enantiocomposition of the mixture in the gas phase (from enantiopure S-PO or R-PO to racemic, or 50:50 S-PO + R-PO), by introducing two hypothesis, namely, that the adsorption is adsorbate-enhanced and that adsorption on adjacent sites requires specific geometries,

Special Issue: Miquel B. Salmeron Festschrift

Received: March 8, 2017

Revised: April 14, 2017

Published: April 28, 2017

different for the homo- versus heteropairs of chiral molecules. Second, the model was shown to also account for the kinetic behavior seen in experiments with sequential exposures of the surface to gas mixtures of different enantiocompositions. Finally, semiquantitative agreement was obtained with data from experiments that show the ability of small amounts of chiral “seeds” to induce enantioselectivity in the adsorption of prochiral molecules such as propylene (Py). These ideas are expanded and discussed further below.

2. METHODOLOGY

2.1. Theoretical Background. Stochastic formulations of kinetic processes are based on the so-called Master equation^{25–28}

$$\frac{dP(\mathbf{x}, t)}{dt} = \sum_{\mathbf{x}' \neq \mathbf{x}} [w_{\mathbf{x}' \rightarrow \mathbf{x}} P(\mathbf{x}', t) - w_{\mathbf{x} \rightarrow \mathbf{x}'} P(\mathbf{x}, t)] \quad (1)$$

where $P(\mathbf{x}, t)$ is the Grand Probability Function, a multidimensional function that describes the probability of finding the system at a particular overall configuration \mathbf{x} (a multidimensional vectorial quantity that includes all possible degrees of freedom of the system) at a given time t , and $w_{\mathbf{x}' \rightarrow \mathbf{x}}$ corresponds to the probability for the conversion of configuration \mathbf{x}' into configuration \mathbf{x} at a given time t . This equation does assume that the processes are Markovian, that is, that the individual events occur independently of each other, but otherwise it provides an exact description of the time evolution of the system, with any of its inherent fluctuations (something that mean-field methods do not cover). Unfortunately, this deceptively simple equation is impossible to solve in most cases.

A simplification of the Master equation is therefore needed to make it practical. Many Monte Carlo methods, including ours, rely on a formalism introduced by Gillespie^{8,29} in which eq 1 is converted into a series of events, the sequence of which is determined by the following equations:

$$\sum_{i=1}^{j-1} R_i \leq r_a R_T < \sum_{i=1}^j R_i; \quad R_T = \sum_{i=1}^m R_i \quad (2)$$

and

$$\tau = \frac{-1}{R_T} \ln(r_b) \quad (3)$$

In these, the overall process under consideration consists of m possible reactions i , the rates of which are given by R_i ; R_T is the sum of all of those rates. Two random numbers r_a and r_b are generated to identify the next in the sequence of events and the time elapsed during that event, respectively: Equation 2 yields a value for j , which corresponds to the event to take place, and equation 3 calculates τ , the associated time increment. These calculations are repeated in order to determine the overall sequence of events that describe the evolution from the initial to the final state of the system.

A few additional considerations have been added to our Monte Carlo algorithm to adapt the Gillespie formalism to our application, to describe adsorption processes on solid surfaces:

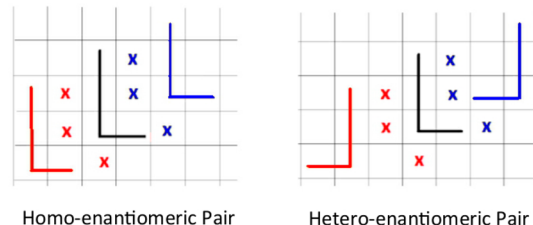
1. The solid surface is represented by a lattice, which is encoded as a matrix. This approach is attributed to Bortz and co-workers,³⁰ and has been used successfully by several groups in the past;^{11,31–47} we have employed it to explain the kinetics of the conversion of CO + NO mixtures on rhodium surfaces, which were found to

involve the formation of islands of N(ads) species and a N–NO(ads) intermediate,^{1,48–54} and also to account for the unique adsorption trends seen during the adsorption of propylene oxide on Pt surfaces modified with 1-(1-naphthyl)ethylamine, used to add enantioselectivity to catalysis.⁵⁵

2. Because the step that determines the time evolution of the system is the impinging frequency of the incoming molecules, which is proportional to their (constant) pressure, the time increment τ per event is expected to be the same for all events (actually, there is a small fluctuation around the average value introduced by the value of r_b in eq 3, but that cancels out when considering many events). Therefore, no explicit accounting of the time is carried out in our simulation (we do not use eq 3). Instead, the passing of time is followed by counting the events.
3. Accordingly, the rates of individual events, which in this case are either the bonding of the incoming molecules to the surface or their bouncing off back into the gas phase, are described by relative probabilities, P_i , rather than reaction rates, R_i . The same eq 2 applies to these, though. In our case, we calculate the probabilities needed to choose the next event in a hierarchical way, by first determining the adsorption site and the type and orientation of the adsorbate and then choosing the type of event that takes place (adsorption versus return to the gas phase). More details about this approach are given below.

2.2. Monte Carlo Algorithm. An algorithm was developed on the basis of the Monte Carlo protocol described above to simulate the uptake of chiral molecules on surfaces. The adsorbates, either propylene oxide (PO) or propylene (Py), are represented by four squares arranged in an “L” shape, as shown in Figure 1. The surface is represented by a square lattice with

Adsorption When a “Safe Zone” Site Is Selected



Homo-enantiomeric Pair Hetero-enantiomeric Pair

Figure 1. Schematic representation of the adsorption geometries proposed for both propylene oxide (PO) and propylene (Py) on the square lattice used in our Monte Carlo algorithm. Each molecule is represented by a four-squares “L”-shaped unit. The blue and red x's in the diagram represent the two sets of sites within the so-called “safe zone” of the initial adsorbate (the black “L” in the diagram) relevant to further molecular uptake on the surface; new adsorbates hitting those sites are directed to the adsorption sites and adsorption geometries indicated by the associated blue and red L's, respectively. A different geometry is required for homochiral versus heterochiral pairs, as indicated by the left and right panels, respectively.

periodic boundary conditions, the evolution of which is followed by using a matching $S(N, N)$ matrix (N being the number of adsorption sites along each dimension). Empty sites, without adsorbate, are represented by 0's, filled sites by 1's (or a series of chosen values if the goal is to differentiate among the different types of adsorbates, S-PO versus R-PO, S-Py versus R-Py, or PO adsorbed at different stages of the experiment),

and sites adjacent to occupied sites, those indicated by the “x” symbols in Figure 1 (which we will call “safe zone” sites), by 2’s. Two additional parameters, P_{empty} and P_{full} , were introduced to provide the probabilities of adsorption on empty and full, or “safe zone”, surface sites, respectively. The following values were used in the simulations reported below:

For PO:

$$P_{\text{empty}} = 1\% \quad \text{and} \quad P_{\text{full}} = 99\%$$

For Py:

$$P_{\text{empty}} = 5\% \quad \text{and} \quad P_{\text{full}} = 95\%$$

The interpretation of these parameters is as follows: with PO, for instance, if an empty site is selected, there is a 1% probability (P_{empty}) for that event to result in adsorption versus a 99% probability ($100\% - P_{\text{empty}}$) for the molecule to bounce back into the gas phase (leading to no changes on the surface). In contrast, if a “safe zone” site is chosen instead (any of the “x” sites in Figure 1), the probability for adsorption is 99% (P_{full}), and that of bouncing back to the gas phase 1% ($100\% - P_{\text{full}}$). Also, when a “safe zone” site is chosen, the new adsorbate is actually reoriented and displaced to one of the new sites and geometries indicated by the red and blue “L” shapes in Figure 1 (depending on the color of the “x” site selected). As indicated there, different adsorption geometries need to be adopted by the incoming molecules depending on their chirality relative to that of the adsorbate already present on the surface (the black “L”).

The flow diagram of the basic Monte Carlo algorithm, shown schematically in Figure 2, consists of the following steps:

1. Inputting of the values for N , the size of the surface matrix $S(N, N)$, the type of the molecule being considered, either PO or Py, and their chirality, either enantiopure ($S\text{-PO}$ or $R\text{-PO}$) molecules or racemic mixtures.
2. Initialization of the system, by setting the event counter n to 1, the counter of the number of occupied sites A to zero, and all $S(X_j, Y_k)$ values to zero, for $j = 1$ to N and $k = 1$ to N . For racemic mixtures, two counters A_1 and A_2 are used to follow the uptake of the two enantiomers separately, and in multistage runs, these are also followed by using independent $A_\#$ parameters.
3. Starting of an event. For this, four random numbers with values between 0 and 1, r_1, r_2, r_3 , and r_4 , are chosen and used to select:
 - a surface site $S(X_1 = \text{Integer}(N \cdot r_1), (Y_1 = \text{Integer}(N \cdot r_2))$
 - the orientation of the incoming molecule, out of four possible choices (up, down, right, left), $O = \text{Integer}(4 \cdot r_3)$
 - the chirality of the molecule, S or R , if racemic mixtures are being considered for PO or if the adsorbate is Py, $C = \text{Integer}(2 \cdot r_4)$.
4. Calculation of the coordinates of the four surface sites to be initially considered for the adsorption of the incoming molecule, $S(X_i, Y_i)$ ($i = 1\text{--}4$), based on the chosen $S(X_1, Y_1)$ matrix position, which is assigned to the kink in the “L” shape of that molecule; the other coordinates are defined relative to the initial (X_1, Y_1) pair by the chosen values of O and C .
5. Decision of the type of event to take place:
 - a. If any of the four positions calculated above are occupied, that is, if any of the corresponding

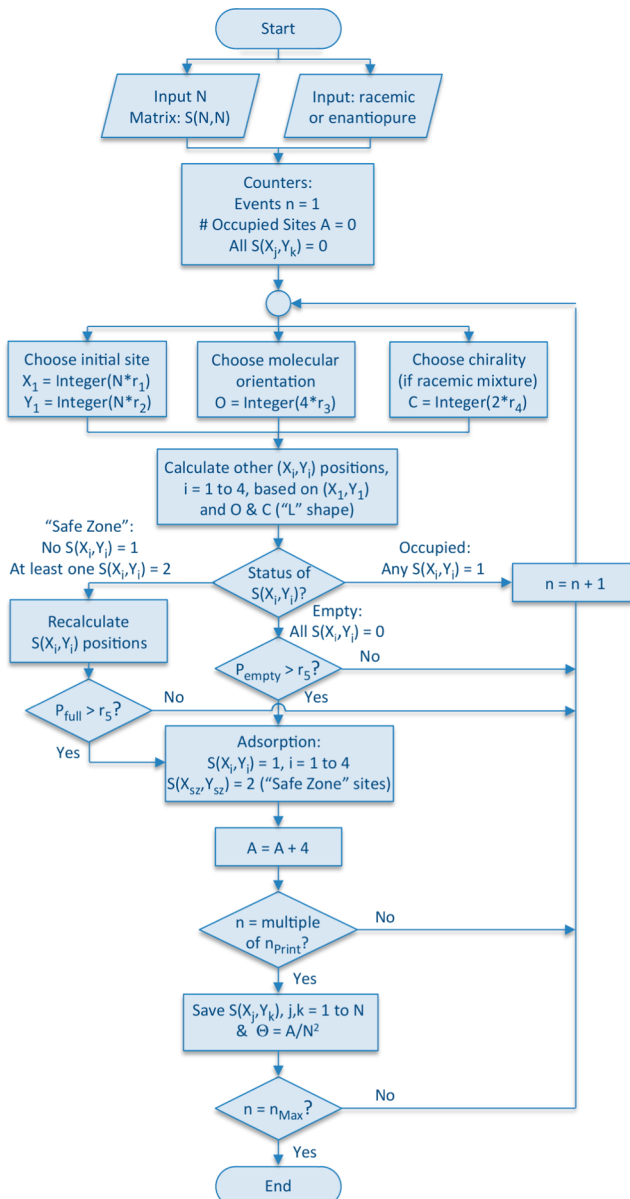


Figure 2. Flow diagram of the Monte Carlo algorithm used for the kinetic simulations on the uptake of chiral molecules on solid surfaces reported here. The calculations were designed to reproduce the experimental results previously published for the uptake of PO on Pt(111).

$S(X_i, Y_i)$ values are one, the event is considered to not result in adsorption. The counter is updated ($n = n + 1$), and another event is initiated.

- If all four positions are empty and are not adjacent to any other adsorbates, in which case the $S(X_i, Y_i)$ values are all zero, the event is considered further for adsorption. A new random number r_5 is generated and compared to P_{empty} to decide if an adsorption event is to take place. If $P_{\text{empty}} \leq r_5$, the answer is no, the counter is updated, and another event is initiated. Otherwise, that is, if $P_{\text{empty}} > r_5$, an adsorption event is assumed to take place, the values for the four chosen $S(X_i, Y_i)$ sites are changed to 1’s, the corresponding “safe zone” positions $S(X_{sz}, Y_{sz})$ are updated to 2’s, and the occupied sites counter is

increased by a value of 4 (to account for the four new sites that have become occupied by the new adsorbate).

- c. If none of the four sites chosen are occupied (all $S(X_i, Y_i) \neq 1$) but at least one is a “safe zone” site ($S(X_i, Y_i) = 2$), the $S(X_i, Y_i)$ positions are recalculated according to the scheme in Figure 1, and a similar process as in point b is then followed, except that P_{full} instead of P_{empty} is used to determine if the event will ultimately result in an adsorption (this will be the case only if $P_{\text{full}} > r_5$). Again, it needs to be remembered that in this case the final adsorption site and adsorption geometry are not the same as those determined initially, during the selection of the values of X_1 , Y_1 , and O .
- 6. A new event is started. These cycles are repeated until no more adsorption is possible, or after reaching a predetermined coverage (in the cases where two or three sequential exposures are considered, as discussed below). Data are saved periodically during these calculations, every n_{Print} events, in the form of a snapshot of the surface matrix $S(X_j, Y_k)$, $j = 1$ to N and $k = 1$ to N , and the values of the number of events n and the number of occupied sites A . The latter is used to calculate the evolution of the surface coverage, $\theta = A/N^2$.

3. RESULTS AND DISCUSSION

3.1. Propylene Oxide Uptake. The first step in this study has been to look into the uptake of propylene oxide (PO) on the surface, to compare with the experimental results we have published previously.²³ Two separate Monte Carlo kinetic runs were performed, with enantiopure S-PO and with a racemic mixture (Rac-PO, 50:50 S-PO + R-PO). The results of those calculations are presented in Figure 3 in the form of the surface

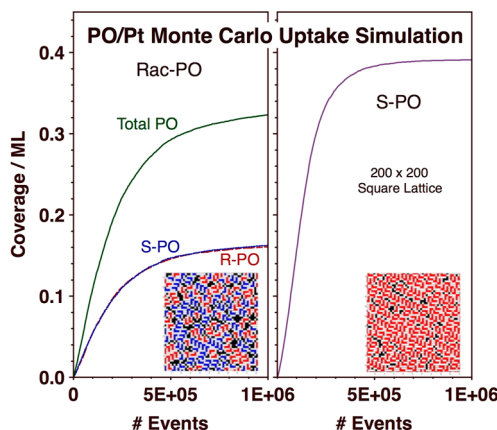


Figure 3. Uptake curves for the adsorption of racemic (left panel) and enantiopure (right) propylene oxide, in the form of surface coverage versus the number of events executed in the Monte Carlo simulations. The individual time evolution of the uptake of the S-PO and R-PO molecules is also provided for the case of the racemic mixture. The insets display snapshots of a section of the final surfaces. In those, the blue and red squares indicate S-PO and R-PO adsorbates, respectively, the white squares the so-called “safe zone” sites, and the black squares unfilled sites.

coverages of each type of adsorbate as a function of the number of events considered. Also reported there are snapshots of a

segment of the final surfaces, showing the adsorbed molecules (“L” shapes in red and blue for S-PO and R-PO, respectively), the “safe zone” sites (white), and the remaining empty sites (black). The most obvious observation from the data in Figure 3 is that the final coverage reached with S-PO is significantly higher than that with Rac-PO, a difference of approximately 20% (the figure does not show the end point, which required many more events to reach, but the trend is clear). This matches what we have reported before on the basis of results from TPD, molecular beam, and STM experiments.^{23,24} Also consistent with the experimental results is the fact that the layers do not adopt any specific long-term order but do seem to form small clusters, typically small linear rows. For the case of the racemic mixture, no significant differences were measured in the uptake of S-PO versus R-PO.

The uptake curves were converted into plots of sticking probabilities versus exposure via derivation of the raw data. Both scales in the new plots, reported in Figure 4, were then

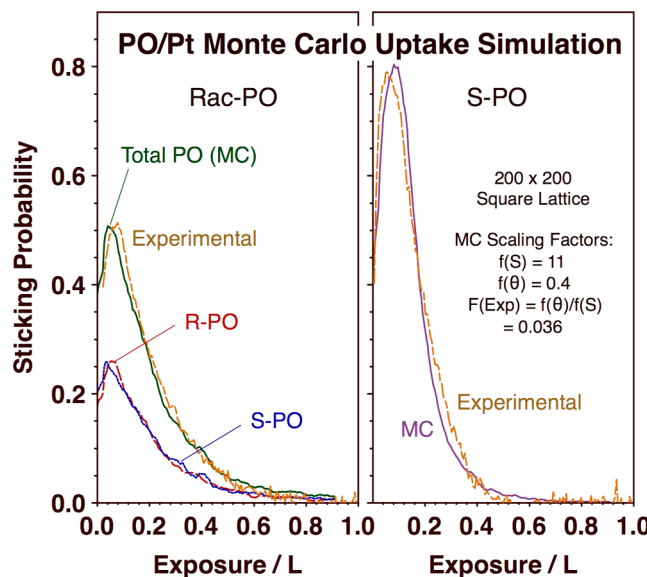


Figure 4. Uptake data in the form of sticking probability versus exposure for the same cases reported in Figure 3. The values of both parameters were scaled appropriately, as discussed in the text, to match the experimental data, which are reported as dashed ochre lines. Good agreement was obtained between the experiments and the simulations, and key features such as the higher sticking probabilities and final coverages with S-PO than with Rac-PO and the initial increase in sticking probability with exposure were nicely reproduced.

recalibrated to better compare with the experimental results (also reported in Figure 4, ochre dashed lines). First, the saturation coverage for pure S-PO obtained with the Monte Carlo simulations, $\theta_{S\text{-PO},\text{sat},MC} = 0.4$, was rescaled to match the experimental value, $\theta_{S\text{-PO},\text{sat},Exp} = 0.16$ ($F_{\theta_{\text{sat}}} = \theta_{S\text{-PO},\text{sat},Exp}/\theta_{S\text{-PO},\text{sat},MC} = 0.4$).²³ The discrepancy between these two values is easy to understand, since here we refer to the coverages in terms of the fraction of the surface sites that are occupied; if expressed in terms of adsorbed molecules per surface square, the simulated saturated coverage would be 0.1 ML instead (since each molecule takes four squares). Also, a correction would need to be made to convert the coverages obtained from the simulations, which use a square lattice, into values consistent with the hexagonal Pt(111) surface used in the experiments. Lastly, the final saturation coverage in the simulations is

contingent on the total footprint chosen for each molecule; it would be relatively straightforward to change the range of the “safe zone” around the adsorbates to modify the final total coverage possible.

The simulated sticking probabilities were also rescaled, by a factor of $F_s = 11$, to match the experimental results. The reason for the low values obtained in the simulations is the small number chosen for P_{empty} , the probability for a molecule impinging on an empty site to stick rather than bounce back to the gas phase. This was required in order to justify the initial rise in sticking with exposure seen experimentally, as discussed below, and it is not easy to change. What we believe is missing in our simulation is the inclusion of a weakly adsorbed precursor state capable of sampling a few surface sites before desorbing if no adsorbates are found in that incursion (and the requirement for P_{empty} is not fulfilled). Such an approach can be implemented in the Monte Carlo routine in a straightforward way, as we have shown before,^{9,56} but a prediction of the outcome of such addition is not trivial. Another potential consideration is the fact that the overall uptake may become faster if the “safe zone” around the adsorbates is enlarged, as mentioned above, because the probability for sticking on those is high. In any case, the low values for the sticking probabilities obtained here are certainly a shortcoming of our simulations, and an issue that requires further exploration. Finally, surface exposures, which are here expressed in Langmuirs ($1 \text{ L} = 1 \times 10^{-6} \text{ Torr}\cdot\text{s}$), were recalibrated accordingly, by using the new scales for both the saturation coverages and the sticking probabilities ($F_{\text{exp}} = F_{\theta_{\text{sat}}} / F_s$).

After such scale calibrations, the results from the Monte Carlo simulations were found to match those obtained experimentally quite well. Several observations are worth highlighting from Figure 4. First, the sticking probabilities in all cases increase with exposure in the initial stages of the uptake, indicating the assistance of adsorbates in the sticking of new incoming molecules. As mentioned before, this phenomenon, which has been reported before for other systems,^{57,58} was reproduced here

by assuming $P_{\text{empty}} \ll P_{\text{full}}$. Second, the specific values of the sticking probabilities for S-PO are much higher than those for Rac-PO during most of the uptake. This order does switch at some point, with a higher preference for adsorption with Rac-PO after approximately 0.25 L, but the change is not sufficient to compensate for the earlier behavior, so the final coverage with S-PO ends up being higher than that with Rac-PO, as mentioned above. Also to note is the earlier peaking (at lower doses) of the sticking probability of Rac-PO compared to that of S-PO. Finally, the curves for S-PO and R-PO are quite similar, certainly within the error bars of our simulations (the traces reported in Figure 4 are actually the average of two runs; several runs were performed to corroborate that the differences seen in the figure between S-PO and R-PO are not real).

3.2. PO Uptake on PO-Precovered Surfaces. Different overall enantiomeric compositions of adsorbates on surfaces can also be obtained by sequentially dosing different enantiomers or enantiomeric mixtures. This approach was tried by us experimentally already, and also resulted in variations in the values of the saturation coverages.^{23,24} The experimental trends in these systems were reproduced here, to a good extent, by our Monte Carlo simulations. Figure 5 summarizes the relevant results from both experiments and simulations where a given (varying) coverage of enantiopure propylene oxide (S-PO in this case, $\theta(\text{S-PO})_{\text{1st}}$) is deposited first, and the surface is then saturated with more S-PO (left panel), R-PO (center), or Rac-PO (right). The first set (S-PO + S-PO) always yields the same final saturation coverage, as expected, since they all are essentially the same experiment (saturation with S-PO, only that the dosing is split in two stages), and is provided here for reference and to illustrate the level of uncertainty associated with the results from our simulations. In the other two cases, however, the final saturation coverage of PO on the surface varies, by up to approximately 20%.

The Monte Carlo simulations for the case of S-PO + Rac-PO sequential dosing (Figure 5, right) yields very similar results to those measured by TPD or molecular beam experiments.

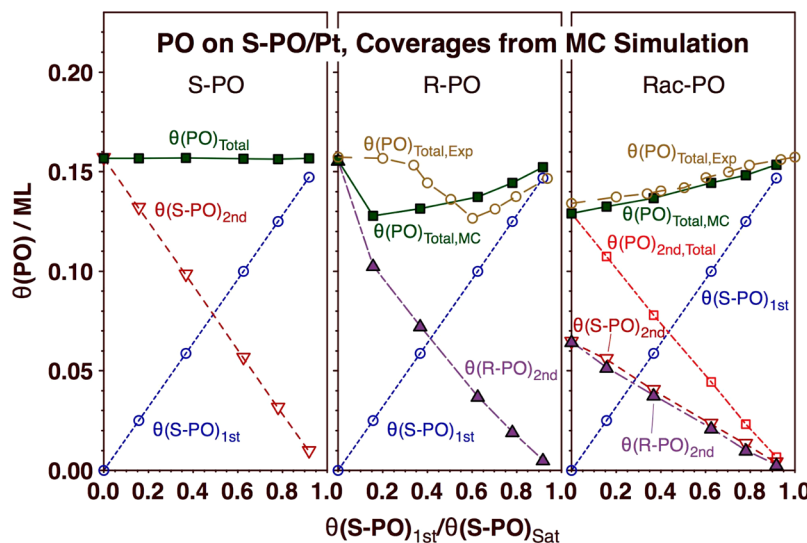


Figure 5. Final coverages obtained from simulations of sequential uptakes of propylene oxide with different chiralities (the experimental data are reported as ochre open circles). In these calculations, the surface was first dosed with varying amounts of S-PO, as indicated in the X axis, and then saturated with more S-PO (left panel), R-PO (center), or Rac-PO (right). It is clear that the coverages reached at saturation vary depending on the sequence of events chosen, even if the exact combination leading to the minimum in saturation coverage with the S-PO + R-PO sequence was not well predicted by the simulations.

The panel for the S-PO + R-PO (Figure 5, center), however, does show a significant discrepancy: the saturation coverage drops in both cases by similar amounts, but the minimum value is reached at different values of the initial coverage of S-PO ($\theta(S\text{-PO})_{1\text{st}}$). Experimentally, that minimum occurs when the overall enantiocomposition of the adsorbed PO layer is closed to racemic, as in the third case (S-PO + Rac-PO), but in the Monte Carlo simulations, it happens almost immediately after a small amount of S-PO is predosed on the surface ($\theta(S\text{-PO})_{1\text{st}} \sim 0.16 \text{ ML}$). We believe that this difference is due to the fact that in the simulations there is no surface diffusion of the adsorbed species once they bind to the surface; in reality, some surface mobility may be possible (and likely).

The evolution of the uptake with the two-step dosing sequence in the Monte Carlo simulations can be visualized in the snapshots of the surface grid obtained after the end of the different PO uptake runs, which are reported for some representative cases in Figure 6. The top row of Figure 6 corresponds to the first four points in the left panel of Figure 5 (the molecules are shown as red "L"-shaped elements). As indicated before, these runs all yield the same final coverage because they all correspond to saturation of the surface with pure S-PO, and that is what is seen in the surface images as well. In the other two cases (S-PO + Rac-PO and S-PO + R-PO, shown in the middle and lower rows, respectively), however, a transition to more mixed layers is observed, with a limited but visible degree of homochiral segregation in the form of linear rows of homochiral molecules (S-PO or R-PO) a few elements in length (the red and blue "L"-shaped elements represent individual S-PO and R-PO molecules, respectively). What seems clear is that, in the S-PO + R-PO case, the initial addition of a few S-PO molecules on the clean surface seems to disrupt the ability of the R-PO added to form such linear arrangements afterward, and appears to create a few dislocations leading to

the formation of isolated spaces inaccessible to future incoming PO molecules (black squares). This may be the explanation for the asymmetry seen in the curve shown in the center panel of Figure 5, an effect that may not be real. Some adsorbate mobility should be added in the Monte Carlo simulations to better reflect the experimental behavior (with the caveat that the runs would take longer times to reach saturation).

The ability to label and track the S-PO ad R-PO molecules on the surface independently in the Monte Carlo simulations, as illustrated in Figure 6, also affords further analysis of the enantioselectivity of the different systems at the various stages of the uptake. Some of the data extracted from such analysis are provided in Figure 7. The open green squares (plus solid line) in that figure correspond to the ratio of the second-stage uptake of S-PO ($\theta(S\text{-PO})_{2\text{nd}}$) relative to that of R-PO ($\theta(R\text{-PO})_{2\text{nd}}$) in the runs with Rac-PO after depositing a given (variable) coverage of S-PO ($\theta(S\text{-PO})_{1\text{st}}$) in the first phase. If the system were to exhibit no enantioselectivity, that ratio should always be 1, since that is the ratio of the PO molecules in the gas phase. Instead, it is clear that there is a slight preference for the uptake of additional S-PO on S-PO-dosed surfaces, a preference that becomes larger with increasing initial $\theta(S\text{-PO})_{1\text{st}}$. This effect is a consequence of the different relative geometries that adjacent adsorbed PO molecules adopt with respect to each other with homo- versus hetero-chiral pairs, as shown in Figure 1.

The same conclusion can be reached when comparing the final PO surface coverages reached in the S-PO + S-PO versus S-PO + R-PO cases. The filled blue diamonds (and long-dashed line) in Figure 7 illustrate this difference by showing a clear deviation from unity in the ratio of the final coverages reached in both of those cases, a trend that is also evident from simple visual comparison of the saturation coverage trends reported in the left versus center panels of Figure 5. The effect would seem to become less pronounced as the initial S-PO coverage is

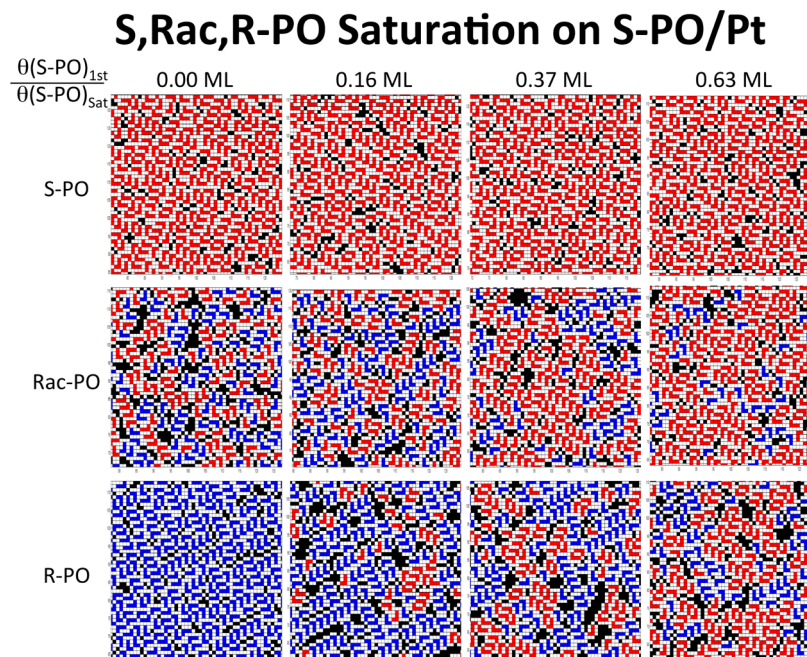


Figure 6. Snapshots of the final surfaces obtained from simulations of propylene oxide uptakes in two-step runs such as those reported in Figure 5. Shown are the surfaces obtained after first dosing varying amounts of S-PO (in increasing order from left to right) and then saturating the surface with more S-PO (top row), Rac-PO (center), or R-PO (bottom). Legend: red = S-PO, blue = R-PO, white = "safe zone" sites, and black = empty sites.

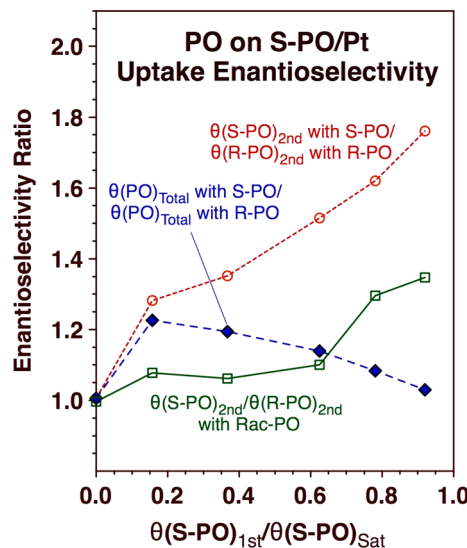


Figure 7. Enantioselectivities calculated from the results of the simulations reported in Figures 5 and 6. Three sets of data are displayed here, namely, (1) the ratio of the coverages of S-PO versus R-PO adsorbed during the second stage of the experiment when Rac-PO is used in that step (green open squares, solid line); (2) the ratio of the coverages of S-PO versus R-PO adsorbed during the second stage of the experiment when using S-PO versus R-PO, respectively (red open circles, short-dashed line); and (3) the ratio of the total PO saturation coverages reached when dosing the surface with S-PO versus R-PO in the second stage of the runs, respectively (blue solid diamonds, long-dashed line). The last two sets of data show how the enantioselectivity for homopairing, that is, for the preferential adsorption of S-PO rather than R-PO next to a S-PO adsorbate, intrinsically increases with increasing initial S-PO coverage but also highlight how that effect is somewhat compensated by the fact that there are less empty sites to fill in the second stage of the uptake with increasing doses in the first.

increased, but that is because doing so leaves a lower number of empty sites for the second phase of the uptake. If the same effect is estimated on the basis of the enantioselectivity of the uptake on the second phase alone (which can be calculated from the Monte Carlo simulations but not in the experiments, unless isotope labeling is used), it is clear that the ratio, $[\theta(S\text{-PO})_{2\text{nd}} \text{ with S-PO}] / [\theta(R\text{-PO})_{2\text{nd}} \text{ with R-PO}]$, increases with increasing $\theta(S\text{-PO})_{1\text{st}}$ and reaches a value close to 2 toward the end of the uptake. This is a significant difference, given that it does not come from any intrinsic changes in chemical interactions, energetics, or even kinetic constants, between the S-PO/S-PO and S-PO/R-PO pairs.

4. AMPLIFICATION OF SURFACE ENANTIOSELECTIVITY WITH PROCHIRAL ADSORBATES

These experiments were also extended to explore the possibility of enhancing the enantioselectivity of surfaces by using so-called “prochiral” molecules, that is, molecules such as propylene (Py, the one used in these studies) that are not chiral by themselves but that become chiral upon adsorption on a surface because of the ensuing break in symmetry. If propylene is adsorbed on a flat solid surface, it can do so in one of two possible chiral configurations (S-Py or R-Py), but because those are identical in every respect other than the fact that they are not superimposable, the expectation is that, probabilistically, the surface would end up with a 50:50 distribution of them. However, it may be possible to bias that even split by using a

small amount of chiral “seeds”. For instance, it has been shown that, on Cu(110), the addition of a small amount of tartaric acid, a chiral molecule, to a monolayer of succinic acid, which is prochiral, leads to a switch from a combination of domains of both chiralities to the dominance of one chirality over the whole surface.²⁰ That effect is believed to be driven by thermodynamics, since the molecules involved are quite mobile on the surface and can rearrange to respond to the new energetic driving force introduced by the chiral “impurity”, but enantioselective adsorption may also be driven kinetically on surfaces where bonding is stronger and surface adsorbate rearrangements more difficult.

We believe that such kinetic adsorption enantioselectivity is what we have seen in our report regarding the adsorption of Py on Pt(111) surfaces predosed with PO.^{19,21} The experiments in that study involved three stages, namely, (first) the adsorption of a small amount of a chiral “seed”, in our case enantiopure PO (S-PO or R-PO); (second) the amplification of the enantioselectivity of the surface via the adsorption of submonolayer coverages of Py on the chirally seeded surface; and (third) the saturation of the surface with a chiral probe, S-PO or R-PO. The experiments are run in pairs, separately with the S-PO and R-PO probes in the third stage, respectively, and the results contrasted to determine the enantioselectivity of the surface. It was shown experimentally that the final uptake (third stage) of PO is different with S-PO versus R-PO, indicating that there is indeed a level of enantioselectivity in the ability of the PO + Py chirally modified surface to further adsorb chiral molecules. It was also demonstrated that the extent of this enantioselectivity increases with the addition of Py to the surface. However, because the seed and probe molecules used are the same (PO in both cases), the information extracted from the TPD and molecular beam results has been somewhat limited. Monte Carlo simulations can help better understand the observed behavior.

Figure 8 displays typical results from Monte Carlo simulations of the three-stage PO + Py + PO dosing procedure used experimentally, in the form of snapshots of the resulting surfaces as a function of the relative coverages of adsorbates added in each step. The sequence shown corresponds to runs where variable amounts of S-PO were dosed first, after which a fixed amount of Py (0.15 L exposure) was added. One powerful feature of the Monte Carlo simulations is that the identity of each type of molecule can be followed: in this case, the initial S-PO molecules are colored red, the S-Py and R-Py that adsorb in the second stage are colored blue and purple, respectively, and the S-PO and R-PO titrants (third stage) are colored orange and green, respectively. Several qualitative trends can be seen in Figure 8. For one, there is a clear increase in Py uptake with increasing coverage of the S-PO seed on the surface, in spite of the fact that the Py dose is the same in all of these experiments. This is because it is significantly more probable for a Py molecule to stick to the surface if it hits a site adjacent to an adsorbed PO molecule (95%) than if it hits an empty site (5%), so starting from a higher S-PO coverage leads to an increase in Py coverage as well. It can clearly be seen that most of the adsorbed Py molecules are in sites adjacent to a preexisting PO adsorbate.

In addition, there is a clear bias toward the uptake of Py in the same chirality as the PO seed directing the adsorption (when the adsorption event is adsorbate-assisted): there is a clear excess of S-Py (blue) over R-Py (purple) molecules on all of these surfaces. This difference is mostly built in the

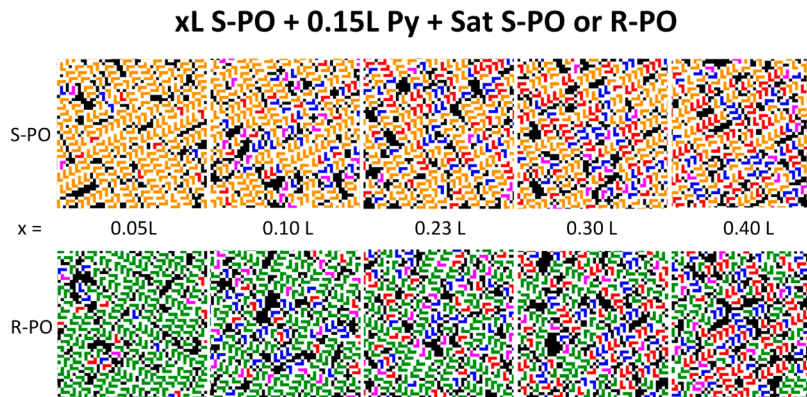


Figure 8. Snapshots of the final surfaces obtained from simulations of three-stage adsorption sequences designed to test the amplification of the enantioselectivity of surfaces using prochiral molecules. In this case, the surface was first chirally seeded by dosing various amounts (x L) of S-PO, then dosed with a fixed amount (0.15 L) of propylene (Py), and finally saturated with either S-PO (top row) or R-PO (bottom). The differences in the uptake in this third stage between the two runs were used to estimate the enantioselectivity of the S-PO + Py-dosed surfaces. Legend: red = initial S-PO, blue = S-Py, purple = R-Py, orange = third-stage S-PO, green = third-stage R-PO.

calculations, since we included a decision step in the simulation where, if the Py molecule is to adsorb next to another preadsorbed molecule, it would do so with a 65% probability of adopting the same chirality and 35% of adopting the opposite chirality. In reality, though, the final enantiobias is even more skewed toward homochirality pairing, by approximately another 5%. This may have to do with the better packing afforded by the homochiral arrangement on the surface, with the formation of linear chains of molecules in the diagonal directions that can be identified even by simple visual inspection.

Additional information can be extracted by quantitative analysis of the data from the simulations. For instance, Figure 9 displays the evolution of the coverages of the relevant species in experiments where a fixed coverage of the S-PO seed ($\theta(\text{S-PO})_{\text{1st}} = 0.03 \text{ ML}$) was augmented with varying doses of Py. Two panels are provided, for the results from titration with S-PO (right) versus R-PO (right). Clearly, as the Py coverage increases, the final PO coverage decreases, to add up to approximately the same total saturation coverage (for PO + Py). However, when using R-PO as the probe molecule, a slight decrease is seen with increasing $\theta(\text{Py})_{\text{2nd}}$ matched by the experimental data (shown in faded colors); this is justified in the same way as the differences in saturation coverages with enantiocomposition were explained in the previous cases, with PO only.

The enantiodifferences seen when titrating with S-PO versus R-PO in the third stage of the experiment are better highlighted in Figure 10, which displays those in two forms, as both a ratio (red filled circles and dashed lines) and a difference (blue open squares and solid lines) between the coverages of the S-PO versus R-PO probe molecules. The ratio of those quantities is higher than 1, and the difference is larger than 0. More importantly, both parameters increase with increasing Py dose (or Py surface coverage), indicating that the enantioselectivity of the surface is enhanced with increasing doses of Py after seeding with S-PO. It is clear that seeding does direct the chirality of the adsorption of Py, and with that amplifies the enantiopurity of the adsorbed layer. Figure 10 also shows that the Monte Carlo results match quite well those measured experimentally in our previous studies (shown in faded colors).^{19,21}

Finally, it is interesting to speculate on how the enantioselective-directing ability of chiral adsorbates may affect the uptake of prochiral molecules by themselves, without any predosing of

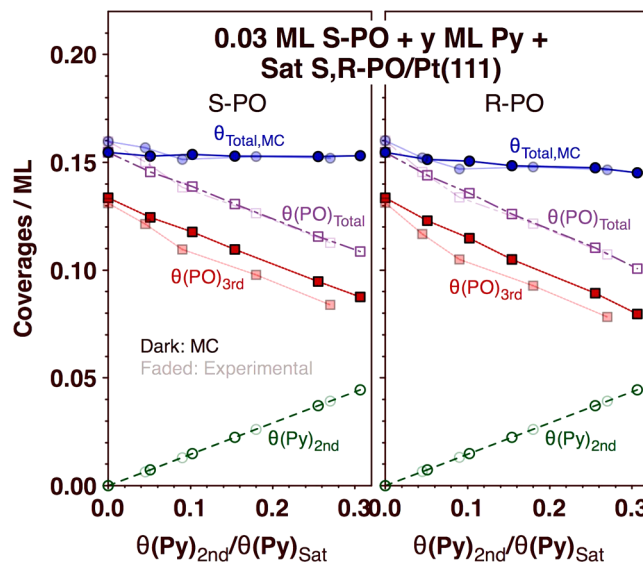


Figure 9. Final coverages calculated from the results of simulations of three-stage experiments similar to those described in Figure 8. Two sets of data are provided, for the use of S-PO (left panel) or R-PO (right) as the probe in the third stage, following the sequential dosing of 0.03 ML of S-PO and varying amounts of Py. The experimental data are provided in faded colors for comparison. The final saturation coverages reached after the third saturation step remain approximately constant with the S-PO probe regardless of the amount of Py used but decrease with increasing Py dose when R-PO is used in the third stage of the experiment instead.

chiral seeds. It should be noted that the uptake of prochiral molecules such as Py on clean surfaces is expected to result in a 50:50 distribution of S-Py and R-Py surface species. However, adsorption next to a preadsorbed Py molecule should be biased, according to our model, toward the chirality of that preexisting adsorbate. To address this issue, we have performed a few preliminary studies on the adsorption of propylene by itself, both experimentally, using a molecular beam setup, and with our Monte Carlo algorithm; Figure 11 compares the results from that work in the form of sticking probabilities versus coverage. It can be seen that the agreement between experiment and simulation is quite good, and that in both cases the sticking probability is approximately constant for the first ~40%

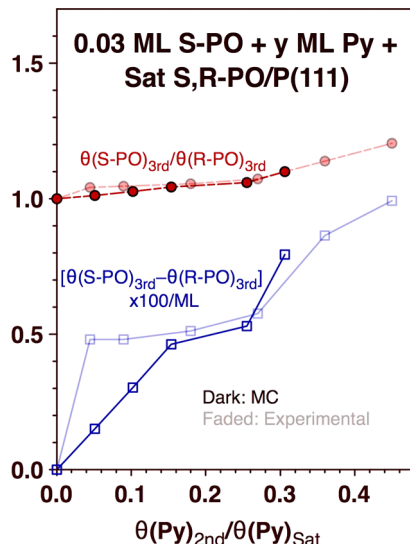


Figure 10. Enantioselectivity of the uptake of PO in the third, probing stage of the runs reported in Figure 9, expressed in two different forms: (1) as a ratio of the amount of S-PO versus R-PO coverage reached in the third stage of dosing (red filled circles, dashed lines) and (2) as a difference (blue open squares, solid lines). The experimental values are provided in faded colors. A clear enantioselectivity enhancement is seen with increasing Py coverage, reflected in both the experimental and simulation results.

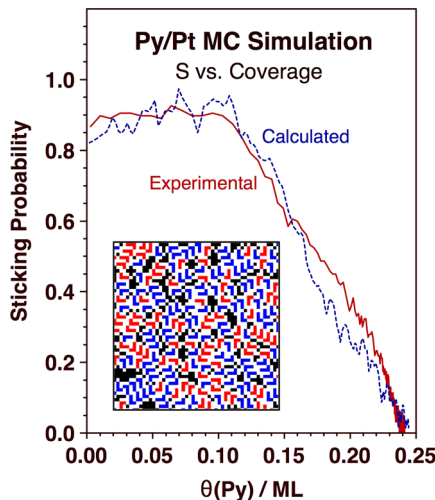


Figure 11. Sticking probability versus coverage for the uptake of Py. The results from a Monte Carlo simulation (blue dashed line) are contrasted with the experimental results from molecular beam measurements on Pt(111) (red solid line); good agreement is seen between the two. The inset shows a snapshot of a section of the final surface, highlighting the preference for one adsorbed Py enantiomer (blue = R-PO) over the other (red = S-PO).

of the uptake, until coverages of approximately 0.1 ML, after which it decreases linearly with increasing coverage. This behavior is typically explained in terms of a mobile precursor adsorption state but was reproduced here simply by relying on the adsorbate-induced adsorption enhancement introduced to explain the initial increase in sticking with coverage seen with PO (Figure 4). The curious result is that, because the same parameters were used in this simulation as in the other cases, with mixed PO and Py doses, the bias toward homopairing on the surface was kept. The consequence of that is an excess of

one enantiomer (*R*-Py) over the other (*S*-Py) on the final surface, depicted in the inset of Figure 11: the *R*-PO:*S*-PO ratio estimated from this simulation is approximately 60:40. If such a result reflects a real effect, it indicates that small fluctuations in the enantiocomposition of the adsorbed layer in the very initial stages of the uptake can be amplified and may trigger measurable enantiobiases later in the saturation layers; this would need to be corroborated experimentally, by STM for instance.⁵⁹ The sensitivity of the kinetic results in the Monte Carlo simulations to the value of the parameter that defines the enantiobias for homopairing on the surface (which was here set to a ratio of 65:35) needs to be tested as well.

5. CONCLUSIONS

The experimental results obtained in previous studies on the uptake of propylene oxide (PO) on Pt(111) were by and large reproduced here quantitatively or semiquantitatively by using a Monte Carlo kinetic algorithm. Several key observations were matched by introducing only a handful of assumptions in the model. First, it was found from TPD, molecular beam, and STM experiments that the saturation coverage of PO on Pt(111) varies with the enantiocomposition of the adsorbed layer, being approximately 20% less dense with racemic mixtures than with one single enantiomer. The sticking probabilities were also measured to be higher with S-PO or R-PO compared to with Rac-PO, and to initially increase with coverage until reaching a maximum value, which occurs at approximately 20% of the uptake. All of these features could be reproduced in the simulations by making the two following assumptions:

- The adsorption is adsorbate-assisted, that is, the sticking probability is higher on a surface site next to an adsorbed molecule than on an empty site.
- The adsorption geometry of an incoming molecule impinging on a site adjacent to a preadsorbed chiral adsorbate is predetermined, and different for incoming molecules of the same versus the opposite chirality to that of the molecule on the surface.

These simulations also show a propensity for the adsorbates to form small linear chains on the surface, a behavior also identified by STM.²³

The same kinetic model and Monte Carlo algorithm were also successful in explaining the amplification of the enantioselectivity of the surface upon dosing a prochiral molecule, propylene (Py) in our case, on substrates already predosed with a small amount of chiral “seeds”, PO in our studies.^{19,21} The same assumptions listed above were needed to account for the behavior of the Py, but, in addition, the adsorbed molecules were set to bias the chirality of the incoming prochiral Py molecules, with a clear preference for adoption with the same chirality as the preadsorbed agent on the surface. This addition not only justifies the amplification of the surface enantioselectivity with Py seen experimentally but also reproduces the uptake of propylene by itself. Intriguingly, our simulations suggest that there may be measurable fluctuations in the enantiocomposition of Py layers on the surface leading to mixtures of adsorbates with a clear preference for one enantiomer. This may be worth checking experimentally.

A couple of limitations were identified in our model that may deserve further investigation in the future. First, we used a square lattice to represent the surface, whereas the Pt(111) substrate employed in the experiments displays a hexagonal pattern. Hexagonal lattices can be easily implemented in future

Monte Carlo simulations. Second, because the intrinsic adsorption probability on empty surface sites was set at a low value, the resulting overall sticking probabilities estimated in the simulations are significantly lower than the experimental values. This was required to highlight the adsorbate-induced adsorption phenomenon that explains the initial increase in sticking probability seen with coverage but needs to be compensated to obtain more realistic results. It may be possible to solve this discrepancy by including a mobile precursor state in the kinetic model, but additional research is needed to test such a hypothesis. The coverages of adsorbates on the surface were also underestimated in our simulations, but that is a much easier problem to solve, requiring only a change in the footprint of the individual adsorbates. Finally, the Monte Carlo algorithm does not reproduce well the trends seen in experiments where molecules of different chirality are dosed sequentially because it does not include any possible adsorbate mobility. The good news is that these and other corrections are relatively easy to add to Monte Carlo algorithms such as that used here. On the positive side, the stochastic approach to kinetics affords the reproduction and explaining of surface phenomena due to heterogeneous and local behavior not captured by mean-field kinetic models.

AUTHOR INFORMATION

Corresponding Author

*E-mail: zaera@ucr.edu.

ORCID

Stavros Karakalos: [0000-0002-3428-5433](https://orcid.org/0000-0002-3428-5433)

Francisco Zaera: [0000-0002-0128-7221](https://orcid.org/0000-0002-0128-7221)

Present Address

[†]S.K.: College of Engineering and Computing, Swearingen Engineering Center, University of South Carolina, Columbia, SC 29208.

Notes

The authors declare no competing financial interest.

ACKNOWLEDGMENTS

This work was supported by the U.S. Department of Energy, Office of Science, Basic Energy Sciences, under Award DE-FG02-12ER16330.

REFERENCES

- (1) Zaera, F. Kinetics of Chemical Reactions on Solid Surfaces: Deviations from Conventional Theory. *Acc. Chem. Res.* **2002**, *35*, 129–136.
- (2) Zaera, F. Kinetics on Model Systems. In *Comprehensive Inorganic Chemistry II*; Reedijk, J., Poeppelmeier, K., Eds.; Elsevier: Oxford, U.K., 2013; pp 39–74.
- (3) Aghalayam, P.; Park, Y. K.; Vlachos, D. G. Construction and Optimization of Detailed Surface Reaction Mechanisms. *AIChE J.* **2000**, *46*, 2017–2029.
- (4) van Santen, R. A.; Markvoort, A. J.; Filot, I. A. W.; Ghouri, M. M.; Hensen, E. J. M. Mechanism and Microkinetics of the Fischer-Tropsch Reaction. *Phys. Chem. Chem. Phys.* **2013**, *15*, 17038–17063.
- (5) Reuter, K. Ab Initio Thermodynamics and First-Principles Microkinetics for Surface Catalysis. *Catal. Lett.* **2016**, *146*, 541–563.
- (6) Önsan, Z. I. Chapter 2: Microkinetic Analysis of Heterogeneous Catalytic Systems. *Multiphase Catalytic Reactors: Theory, Design, Manufacturing, and Applications*; John Wiley & Sons, Inc.: Hoboken, NJ, 2016; pp 17–52.
- (7) Schaad, L. J. The Monte Carlo Integration of Rate Equations. *J. Am. Chem. Soc.* **1963**, *85*, 3588–3592.
- (8) Zaera, F.; Rusinek, I. Monte Carlo Simulation for Inhomogeneous Chemical Kinetics: Application to the Belousov-Zhabotinskii Reaction. *J. Comput. Chem.* **1981**, *2*, 402–409.
- (9) Nordmeyer, T.; Zaera, F. A Monte Carlo Simulation for the Precursor Model of Adsorption of a Spatially Homogeneous Surface. *Chem. Phys. Lett.* **1991**, *183*, 195–198.
- (10) Sales, J. L.; Uñac, R. O.; Gargiulo, M. V.; Bustos, V.; Zgrablich, G. Monte Carlo Simulation of Temperature Programmed Desorption Spectra: A Guide through the Forest for Monomolecular Adsorption on a Square Lattice. *Langmuir* **1996**, *12*, 95–100.
- (11) Hansen, E. W.; Neurock, M. Modeling Surface Kinetics with First-Principles-Based Molecular Simulation. *Chem. Eng. Sci.* **1999**, *54*, 3411–3421.
- (12) Zhdanov, V. P. Monte Carlo Simulations of Oscillations, Chaos and Pattern Formation in Heterogeneous Catalytic Reactions. *Surf. Sci. Rep.* **2002**, *45*, 231–326.
- (13) Chatterjee, A.; Vlachos, D. G. An Overview of Spatial Microscopic and Accelerated Kinetic Monte Carlo Methods. *J. Comput.-Aided Mater. Des.* **2007**, *14*, 253–308.
- (14) Ma, Z.; Zaera, F. Chiral Modification of Catalytic Surfaces. In *Design of Heterogeneous Catalysis: New Approaches Based on Synthesis, Characterization, and Modelling*; Ozkan, U. S., Ed.; Wiley-VCH: Weinheim, Germany, 2009; pp 113–140.
- (15) Mark, A. G.; Forster, M.; Raval, R. Recognition and Ordering at Surfaces: The Importance of Handedness and Footedness. *Chem-PhysChem* **2011**, *12*, 1474–1480.
- (16) Ernst, K.-H. Molecular Chirality in Surface Science. *Surf. Sci.* **2013**, *613*, 1–5.
- (17) Yun, Y.; Gellman, A. J. Adsorption-Induced Auto-Amplification of Enantiomeric Excess on an Achiral Surface. *Nat. Chem.* **2015**, *7*, 520–525.
- (18) Gellman, A. J.; Tysoe, W. T.; Zaera, F. Surface Chemistry for Enantioselective Catalysis. *Catal. Lett.* **2015**, *145*, 220–232.
- (19) Karakalos, S.; Hong, J.; Zaera, F. Changes in the Enantiomeric Composition of Chiral Mixtures Upon Adsorption on a Non-Chiral Surface. *Angew. Chem., Int. Ed.* **2016**, *55*, 6225–6228.
- (20) Ernst, K. H. Amplification of Chirality at Solid Surfaces. *Origins Life Evol. Biospheres* **2010**, *40*, 41–50.
- (21) Karakalos, S.; Zaera, F. Amplification of Enantioselectivity on Solid Surfaces Using Nonchiral Adsorbates. *J. Phys. Chem. C* **2015**, *119*, 13785–13790.
- (22) Shukla, N.; Ondeck, N.; Gellman, A. J. Quantitation of Enantiospecific Adsorption on Chiral Nanoparticles from Optical Rotation. *Surf. Sci.* **2014**, *629*, 15–19.
- (23) Karakalos, S.; Lawton, T. J.; Lucci, F. R.; Sykes, E. C. H.; Zaera, F. Enantiospecific Kinetics in Surface Adsorption: Propylene Oxide on Pt(111) Surfaces. *J. Phys. Chem. C* **2013**, *117*, 18588–18594.
- (24) Gordon, A. D.; Karakalos, S.; Zaera, F. Dependence of the Adsorption of Chiral Compounds on Their Enantiomeric Composition. *Surf. Sci.* **2014**, *629*, 3–10.
- (25) McQuarrie, D. A.; Jachimowski, C. J.; Russell, M. E. Kinetics of Small Systems. II. *J. Chem. Phys.* **1964**, *40*, 2914–2921.
- (26) Laurenzi, I. J. An Analytical Solution of the Stochastic Master Equation for Reversible Bimolecular Reaction Kinetics. *J. Chem. Phys.* **2000**, *113*, 3315–3322.
- (27) Gadgil, C.; Lee, C. H.; Othmer, H. G. A Stochastic Analysis of First-Order Reaction Networks. *Bull. Math. Biol.* **2005**, *67*, 901–946.
- (28) Lee, C. H.; Kim, P. An Analytical Approach to Solutions of Master Equations for Stochastic Nonlinear Reactions. *J. Math. Chem.* **2012**, *50*, 1550–1569.
- (29) Gillespie, D. T. Exact Stochastic Simulation of Coupled Chemical Reactions. *J. Phys. Chem.* **1977**, *81*, 2340–2361.
- (30) Bortz, A. B.; Kalos, M. H.; Lebowitz, J. L. A New Algorithm for Monte Carlo Simulation of Ising Spin Systems. *J. Comput. Phys.* **1975**, *17*, 10–18.
- (31) Silverberg, M.; Ben-Shaul, A. Adsorbate Islanding in Surface Reactions: A Combined Monte Carlo-Lattice Gas Approach. *J. Chem. Phys.* **1987**, *87*, 3178–3194.

- (32) Becker, O. M. Correlated Chemisorption: The Effect of Coalescence and Diffusion on Chemisorption Islands. *J. Chem. Phys.* **1992**, *96*, 5488–5496.
- (33) Jansen, A. P. J. Monte Carlo Simulations of Chemical Reactions on a Surface with Time-Dependent Reaction-Rate Constants. *Comput. Phys. Commun.* **1995**, *86*, 1–12.
- (34) Riccardo, J. L.; Steele, W. A.; Cuesta, A. J. R.; Zgrablich, G. Pure Monte Carlo Simulation of Model Heterogeneous Substrates: From Random Surfaces to Many-Site Correlations. *Langmuir* **1997**, *13*, 1064–1072.
- (35) Raimondeau, S.; Vlachos, D. G. Recent Developments on Multiscale, Hierarchical Modeling of Chemical Reactors. *Chem. Eng. J.* **2002**, *90*, 3–23.
- (36) Zhdanov, V. P.; Kasemo, B. Bistability in Catalytic Reactions on the nm Scale. *Surf. Sci.* **2002**, *496*, 251–263.
- (37) Nieskens, D. L. S.; van Bavel, A. P.; Niemantsverdriet, J. W. The Analysis of Temperature Programmed Desorption Experiments of Systems with Lateral Interactions; Implications of the Compensation Effect. *Surf. Sci.* **2003**, *546*, 159–169.
- (38) Chatterjee, A.; Vlachos, D. G. Multiscale Spatial Monte Carlo Simulations: Multigriding, Computational Singular Perturbation, and Hierarchical Stochastic Closures. *J. Chem. Phys.* **2006**, *124*, 064110.
- (39) Mei, D.; Sheth, P. A.; Neurock, M.; Smith, C. M. First-Principles-Based Kinetic Monte Carlo Simulation of the Selective Hydrogenation of Acetylene over Pd(111). *J. Catal.* **2006**, *242*, 1–15.
- (40) Nagasaka, M.; Kondoh, H.; Nakai, I.; Ohta, T. CO Oxidation Reaction on Pt(111) Studied by the Dynamic Monte Carlo Method Including Lateral Interactions of Adsorbates. *J. Chem. Phys.* **2007**, *126*, 044704.
- (41) Temel, B.; Meskine, H.; Reuter, K.; Scheffler, M.; Metiu, H. Does Phenomenological Kinetics Provide an Adequate Description of Heterogeneous Catalytic Reactions? *J. Chem. Phys.* **2007**, *126*, 204711.
- (42) Mei, D.; Neurock, M.; Smith, C. M. Hydrogenation of Acetylene-Ethylene Mixtures over Pd and Pd-Ag Alloys: First-Principles-Based Kinetic Monte Carlo Simulations. *J. Catal.* **2009**, *268*, 181–195.
- (43) Álvarez-Falcón, L.; Alas, S. J.; Vicente, L. Dynamic Monte Carlo Simulation of the Reaction on Pt(100): TPR Spectra. *Phys. A* **2011**, *390*, 4174–4183.
- (44) Matera, S.; Meskine, H.; Reuter, K. Adlayer Inhomogeneity without Lateral Interactions: Rationalizing Correlation Effects in CO Oxidation at RuO₂(110) with First-Principles Kinetic Monte Carlo. *J. Chem. Phys.* **2011**, *134*, 064713.
- (45) van Santen, R. A.; Ghouri, M. M.; Shetty, S.; Hensen, E. M. H. Structure Sensitivity of the Fischer-Tropsch Reaction; Molecular Kinetics Simulations. *Catal. Sci. Technol.* **2011**, *1*, 891–911.
- (46) Prats, H.; Álvarez, L.; Illas, F.; Sayós, R. Kinetic Monte Carlo Simulations of the Water Gas Shift Reaction on Cu(111) from Density Functional Theory Based Calculations. *J. Catal.* **2016**, *333*, 217–226.
- (47) Hoffmann, M. J.; Engelmann, F.; Matera, S. A Practical Approach to the Sensitivity Analysis for Kinetic Monte Carlo Simulation of Heterogeneous Catalysis. *J. Chem. Phys.* **2017**, *146*, 044118.
- (48) Bustos, V.; Gopinath, C. S.; Uñac, R.; Zaera, F.; Zgrablich, G. Lattice-Gas Study of the Kinetics of Catalytic Conversion of NO-CO Mixtures on Rhodium Surfaces. *J. Chem. Phys.* **2001**, *114*, 10927–10931.
- (49) Zaera, F.; Wehner, S.; Gopinath, C. S.; Sales, J. L.; Gargiulo, V.; Zgrablich, G. Evidence for the Formation of Nitrogen Islands on Rhodium Surfaces. *J. Phys. Chem. B* **2001**, *105*, 7771–7774.
- (50) Bustos, V.; Uñac, R.; Zaera, F.; Zgrablich, G. Lattice-Gas Study of the Kinetics of the Catalytic NO-CO Reaction on Rhodium Surfaces. II. The Effect of Nitrogen Surface Islands. *J. Chem. Phys.* **2003**, *118*, 9372–9379.
- (51) Avalos, L. A.; Bustos, V.; Uñac, R.; Zaera, F.; Zgrablich, G. Toward a Realistic Model for the Kinetics of the NO + CO Reaction on Rhodium Surfaces. *J. Mol. Catal. A: Chem.* **2005**, *228*, 89–95.
- (52) Avalos, L. A.; Bustos, V.; Uñac, R.; Zaera, F.; Zgrablich, G. Dynamic Monte Carlo Simulation of the NO+CO Reaction on Rh(111). *J. Phys. Chem. B* **2006**, *110*, 24964–24971.
- (53) Uñac, R. O.; Bustos, V.; Wilson, J.; Zgrablich, G.; Zaera, F. Molecular Beam Measurements and Monte Carlo Simulations of the Kinetics of N₂O Decomposition on Rh(111) Single-Crystal Surfaces. *J. Chem. Phys.* **2006**, *125*, 074705.
- (54) Zaera, F.; Sales, J. L.; Gargiulo, M. V.; Ciacera, M.; Zgrablich, G. On the Formation of Nitrogen Islands on Rhodium Surfaces. *J. Phys. Chem. C* **2007**, *111*, 7795–7800.
- (55) Sales, J. L.; Gargiulo, V.; Lee, I.; Zaera, F.; Zgrablich, G. Monte Carlo Modeling of the Enantioselective Adsorption of Propylene Oxide on 1-(1-Naphthyl)Ethylamine-Modified Pt(111) Surfaces. *Catal. Today* **2010**, *158*, 186–196.
- (56) Nordmeyer, T.; Zaera, F. A Theoretical Study of the Parameters Affecting the Kinetics of Gas Adsorption on Solid Surfaces. *J. Chem. Phys.* **1992**, *97*, 9345–9354.
- (57) Arumainayagam, C. R.; McMaster, M. C.; Madix, R. J. Coverage Dependence of Molecular Adsorption Dynamics: Ethane on Platinum (111). *J. Phys. Chem.* **1991**, *95*, 2461–2465.
- (58) Bowker, M.; King, D. A. Anomalous Adsorption Kinetics. Γ-Nitrogen on the {110} Plane of Tungsten. *J. Chem. Soc., Faraday Trans. 1* **1979**, *75*, 2100–2115.
- (59) Parschau, M.; Passerone, D.; Rieder, K.-H.; Hug, H. J.; Ernst, K.-H. Switching the Chirality of Single Adsorbate Complexes. *Angew. Chem., Int. Ed.* **2009**, *48*, 4065–4068.